Engineering Chemistry
ISSN: 2813-6535, Vol. 7, pp 71-78
doi:10.4028/p-OI9QmD

Submitted: 2023-12-06
Revised: 2023-12-31
Accepted: 2024-01-02
Online: 2024-06-26

Bilayer Solar Steam Generator by Co-Gelation Method

Annisa Nur Fidyanti Pamuji[1,a], Julianandа[1,2,b], Widiyastuti[1,c], Tantular Nurtono[4,d], Heru Setyawan[1,e*]

[1]Department of Chemical Engineering, Faculty of Industrial Technology, Sepuluh Nopember Institute of Technology, Kampus ITS, Sukolilo, Surabaya 60111, Indonesia

[2]Department of Chemical Engineering, Faculty of Engineering, Brawijaya University, Jalan MT. Haryono 167, Klojen, Malang 65145, Indonesia

[a]fpamujiannisa@gmail.com, [b]julia.nanda@ub.ac.id, [c]widi@chem-eng.its.ac.id, [d]tantular@chem-eng.its.ac.id, [e*]sheru@chem-eng.its.ac.id

Keywords: Solar steam generator, cellulose aerogel, magnetite, co-gelation.

Abstract. The interfacial solar steam generator presents a viable and environmentally conscious solution for generating fresh water from seawater. The interfacial solar steam generator is accomplished through the integration of a photothermal material with a supporting material, resulting in a bilayer structure. In general, the efficiency of achieving a bilayer structure by the coating of a photothermal material on the surface of a substrate is limited. This is due to the potential for separation and variations in coating thickness, which can result in a drop in the rate of evaporation. In this study, a bilayer structure was successfully obtained through the implementation of a co-gelation technique utilizing a biomass-derived substrate, aerogel cellulose, and magnetite (Fe_3O_4) as photothermal materials. Additionally, we investigate the impact of magnetic fields on the evaporation rate of photothermal materials. The bilayer solar steam generator obtained demonstrates a notable evaporation rate of 1.87 $kg.m^{-2}h^{-1}$, which is sufficient to meet the daily water requirements of individuals.

Introduction

The solar steam generator represents a practical and environmentally friendly solution to the global issue of water scarcity. Various technologies, such as technologies based on membrane and thermal energy has been employed for converting seawater into fresh water[1]. Nevertheless, it is important to note that these technologies consume a significant amount of energy, acquire high costs, and are prone to fouling, which ultimately diminishes their energy efficiency[2]. The utilisation of solar steam generators presents a potential solution to address the problem of water scarcity. By using solar radiation as a renewable energy source, these generators have the capacity to be constructed utilising biomass derived materials. This characteristic provides such a cost-effective and sustainable technology for mitigating water scarcity[3]. Solar radiation also have a wide range of application, for example there is research about substituting electricity with solar radiation for charging electrical vehicles in Bali, so the concept of independent powers producer can be achieved [22].

Solar radiation has wide range of applications, including large-scale power generation, desalination systems, etc., depend on the effective harvesting of solar energy for water evaporation or steam generation. However, those applications require high optical concentration of solar radiation and are prone from high optical loss, which are expensive and high maintenance[3]. Heat localization become one of solution to solve those problem without using high optical concentrator[4]. This method can minimize heat losses and simultaneously avoid unnecessary heating bulk water that only consumes energy. The system of heat localization works by using the ability of materials to efficiently absorb light and convert it into thermal energy, as well as their characteristics as thermal insulator, and wicking water towards surface (capillary action)[3].

Bilayer solar steam generator is consisted of photothermal conversion layer and water transport layer we called substrate, and is proved to have better ability to localizes solar radiation, reducing heat losses and enhancing efficiency[4]. The photothermal layer at the surface of the evaporator works as

converter of solar energy from solar radiation for steam generation. The water transfer layer or substrate below the photothermal layer continuously supplying water to surface and effectively reduces heat loss due to its characteristic as thermal insulator, maximizing the heat localization effect [5]. The water wicks to the surface, evaporates and forms vapour which leaves the structure [4].
In this study, we apply the co-gelation approach to build a bilayer solar steam generator with aerogel cellulose as the substrate and magnetite as the photothermal components. Aerogel cellulose has an appealing characteristic of low density and great porosity[6], enabling it to achieve buoyancy. Additionally, it possesses a low thermal conductivity and exhibits excellent capillarity, which are key attributes required for efficient heat localisation in solar steam generators[3]. Magnetite is used as a photothermal material due to its remarkable characteristics, including its high thermal conductivity and its capacity to efficiently absorb and transform solar radiation into thermal energy [7]. The co-gelation method is used to prevent the separation of two components, which has the potential to reduce the evaporation rate of a solar steam generator. Magnet-assisted manufacturing was employed to reduce the amount of photothermal materials used and affecting the evaporation rate [8].

Materials and Methods

Materials. Coir fibers were otabined from Tulungagung, Indonesia. Hydrochloric acid (HCl; 37%; reagent grade) and sodium hydroxide (NaOH; reagent grade) were supplied by Merck. Sodium hypochlorite (NaOCl; 5%) was supplied by Onemed. Ethanol (96%) was supplied from Sigma Aldrich. Urea (CON_2H_4) was supplied by PT. Petrokimia Gresik, Indonesia. Demineralized water was used for all synthesis and treatment processes. All chemicals were used without purification.

Preparation of cellulose pulp. Various treatments were applied to coir fibers to eliminate the hemicellulose and lignin components. The coir fiberss undergoes a process of grinding and sieving using a 150-mesh sieve. The 150-mesh coir fibers were treated to two rounds of acid digestion, employing 1 M and 0.5 M hydrochloric acid (HCl) solutions consecutively. The process of digestion is carried out at a temperature of 85°C for a duration of 30 minutes. The second treatment used 1 M sodium hydroxide (NaOH) alkali solution, which was repeated three times under identical conditions. The final step is the elimination of lignin, which is achieved through the bleaching using natrium hypochlorite (NaOCl) 1.5% solution on two separate processes[9]. The pulp obtained from the procedure is ready for utilization as aerogel cellulose.

Preparation of magnetite (Fe_3O_4). The magnetite (Fe_3O_4) used throughout this study was generated by the electrochemical method, employing a formerly used iron plate and demineralized water as the electrolyte. The synthesis process was conducted under ambient conditions, specifically at room temperature, for a duration of three hours, employing a current of 3 volts[10]. The magnetite (Fe_3O_4) produced is filtered and subjected to a drying process at a temperature of 100°C for one hour, giving it suitable for using as a photothermal material.

Synthesis of bilayer solar steam generator. The pulp obtained from the previous procedure is mixed with a NaOH-Urea solution in an ice bath for a duration of 30 minutes. This solution serves as a crosslinking agent, facilitating the formation of aerogel cellulose. The NaOH-Urea solution used contains 1 gram of NaOH and 4 grams of urea dissolved in 10 mL of demineralized water. To further improve dispersion, the mixture was put through sonication for 10 minutes after the addition of magnetite (Fe_3O_4) as photothermal materials, constituting 10% of the total weight. The mixture was kept to a temperature of -5°C for 24 hours that will encourage the process of co-gelation. In this stage, we introduced a magnetic field as an additional variable to investigate its impact on the evaporation rate. Once the gel had solidified, it was placed under ambient temperature to thaw and coagulated with ethanol (96%) as a coagulant, resulting in the formation of an alcohol-based gel. This gel was left undisturbed for a duration of 24 hours. Following coagulation, the gel formed was submerged in demineralized water to solvent exchange, and process was repeated until the solution's pH was neutral. Afterwards, the sample was kept to freezing at a temperature of -12°C for 24 hours in preparation for the following freeze-drying process. Freeze dry was done at -50°C, 15 bar for 8 hours.

The frozen sample underwent 8 hours of freeze drying. AM-0 stands for bilayer aerogel magnetite without assisted by magnet, and AM-1 stands for magnet-assisted bilayer aerogel magnetite.

Characterization

Density and Porosity Test. The density of cellulose aerogels was obtained from measured mass and bulk volume and porosity of cellulose aerogel was determined from its bulk density using the Eq. 1

$$\phi = 1 - \frac{\rho_b}{\rho_t} \quad (1)$$

where $\rho_b$and ρ_t, respectively, the bulk density of cellulose aerogel and the true density of cellulose (1,528 g/cm^3). The bulk density was determined from the measured mass and bulk volume of cellulose aerogel.

X-Ray Diffraction. The identification of XRD was using X-ray diffractometer (X'pert, Phillips). The light absorption of materials was determined using a light intensity meter (Apogee MQ-500), at 5-90 degrees.

Fourier Transform Infrared Spectroscopy. The identification of functional groups of the samples was analyzed using Fourier transform infrared spectroscopy (FTIR; IR Tracer-100, Shimadzu) with a scanning range of 400−4000 cm^{-1}.

Conductivity Thermal Test.

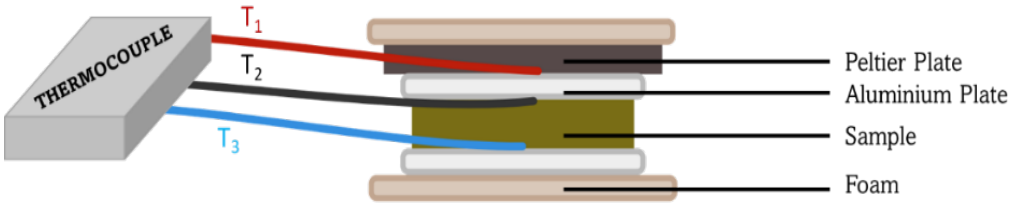

Fig. 1. Conductivity Thermal Test

Conductivity thermal is conducted based on ASTM D5470. This test using peltier plate as heat source, aluminium plate as conductive plate and recording temperature using thermocouple in three points, as in Fig. Conductivity thermal can be calculated by:

$$K_{aerogel} = \frac{P}{h.(T_2 - T_3)} \quad (2)$$

$$P = K_{Al} \times A \times (T_1 - T_2) \quad (3)$$

Where $K_{aerogel}$ is conductivity thermal of bilayer aerogel cellulose with magnetite, P is heat transferred from peltier plate to aluminium plate, h is height of sample, K_{Al} is conductivity thermal of aluminium plate, and T is temperature.

Evaporation Rate. A solar simulator (Toption) is used as light source. All solar steam generation experiments are conducted under room temperature, and the intensity of simulated sunlight controlled at 1 kW.m^{-2} (one sun). Surface temperature and bulk water temperature is monitored and recorded by thermocouple (PicoLog). The mass change of evaporation is determined by electronic balance (CHQ). The evaporation rate (kg.m^{-2}h^{-1}) were calculated by Eq. 3, respectively:

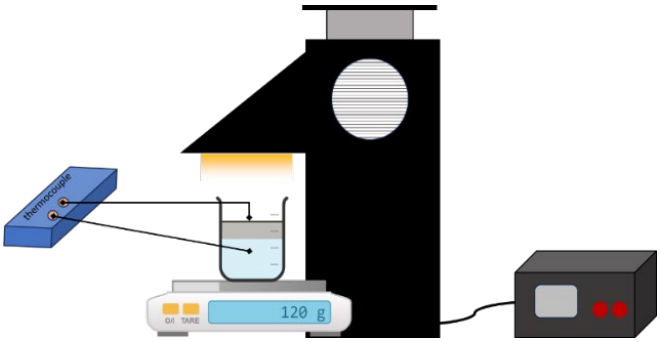

Fig. 2. Evaporation Rate Tests

$$m = \frac{\Delta m}{(A.t)} \quad (4)$$

Where Δm is the mass water of evaporation in 1 h (kg), A is the area of cross section of substrate (m^2), and t is the time of solar irradiation (1 h).

Results and Discussion.

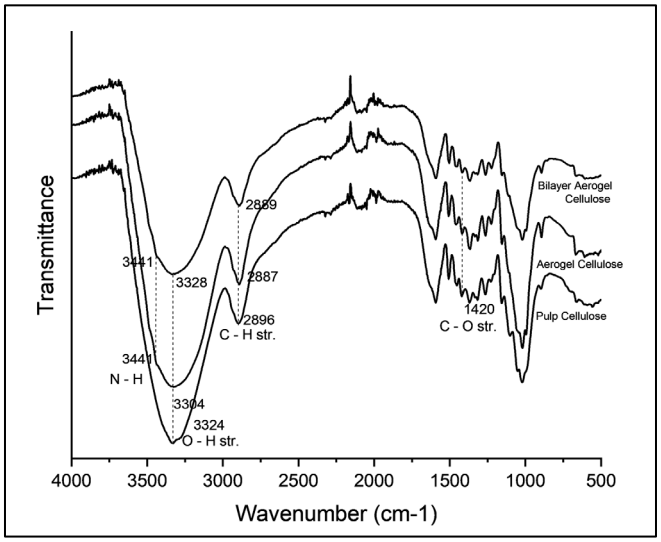

Fig. 3. FTIR Spectra of Bilayer Aerogel Cellulose, Aerogel Cellulose, and Pulp Cellulose

Figure 3 shows the FTIR spectra of three samples: a) pulp obtained after various treatment; b) aerogel cellulose; c) bilayer aerogel cellulose with magnetite. In all samples, it is possible to identify three prominent bands that correlate to cellulose. The band observed at a wavenumber of 3324 cm^{-1} can be related to intramolecular hydrogen bonding, namely the stretching of O-H bonds [11]. On the other hand, the band detected at 2896 cm^{-1} related to the stretching of C-H bonds in the CH and CH_2 groups present in the cellulose molecule [12]. Next, the band at 1420 cm^{-1} are related to C=O carbonyl stretching of acetyl groups in hemicellulose that can be found in lignin compound [12]. However, the band in the samples after being aerogel is shifted to the right. These show that the mixture of NaOH, urea and demineralized water was added as crosslinker agent break up the intra- and intermolecular hydrogen bonding of cellulose and physically caused cellulose swelling in solution [13].

A new band at 3441 cm^{-1} appears in the spectra of samples of aerogel cellulose and bilayer aerogel cellulose with magnetite, which is pulp that has been crosslinked by NaOH and urea. Cellulose is consisted of hydrophobic groups which are glucopyranose ring, and hydrophilic groups which are hydroxyl group. Addition of NaOH solution can disturb hydroxyl group in cellulose, making glucopyranose ring as hydrophobic groups able to form bonds with urea [13], [14]. The band seen in 3441 cm^{-1} can be ascribed to the functional group known as N-H [15]. There is no significant difference between FTIR spectra from aerogel cellulose and bilayer aerogel cellulose with magnetite

because magnetite added are low concentrations (10% total weight), but can be explained in XRD peaks.

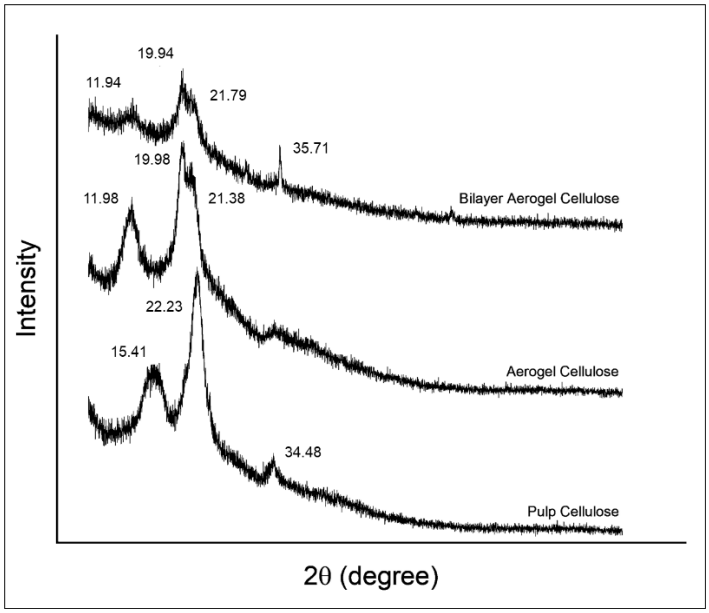

Fig. 4. XRD peaks for Bilayer Aerogel Cellulose, Aerogel Cellulose and Pulp Cellulose

Figure 4 shows the XRD pattern of: a) pulp obtained after various treatment; b) aerogel cellulose; c) bilayer aerogel cellulose with magnetite. The XRD pattern for pulp cellulose have three peaks, 15.86°; 22.51°; 34.45° which identical with patterns of cellulose I [13], [16], [17]. XRD pattern for aerogel cellulose and bilayer aerogel cellulose with magnetite have different peaks at 11.98°, 19.98°, 21.38° which identical with patterns of cellulose II [13], [16], [17]. Dissolution of cellulose into crosslinker agent NaOH–urea at -5 °C followed by gelation results in the change of structure of cellulose I into cellulose II [17], [18]. There are differences between XRD pattern for bilayer aerogel with magnetite, with another peaked found in 35.71° which is one of the peaks of standard magnetite by JCPDS No.19-0629. Peak at 35.71° for bilayer aerogel cellulose is sharper, indicating magnetite that was added have a high crystallinity.

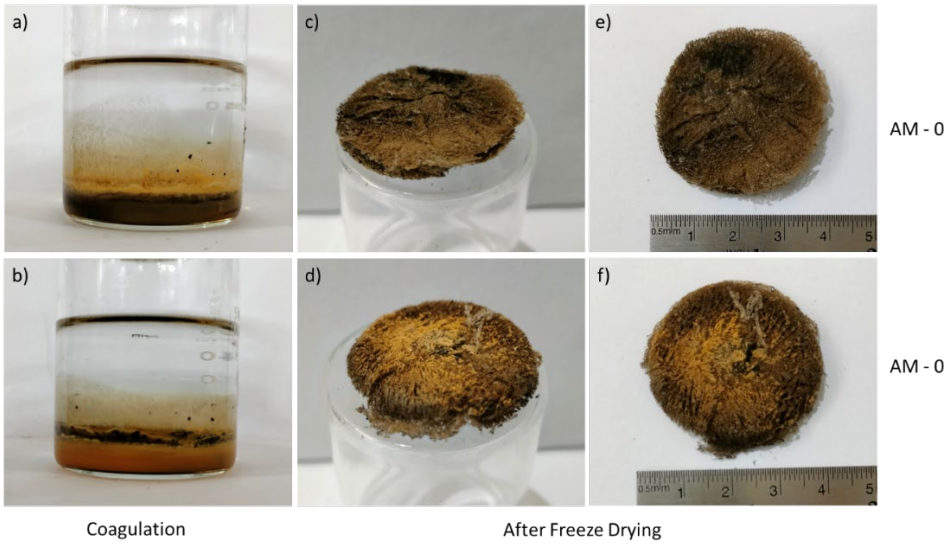

Fig. 5. Photo of AM-0 and AM-1 at different condition

Figure 5 shows the physical appearance of AM-0 and AM-1. AM-0 stands for bilayer aerogel magnetite without assisted by magnet, and AM-1 stands for magnet-assisted bilayer aerogel magnetite. The density of both samples is very low, with AM-0 measuring 0.0067 $g.cm^{-3}$ and AM-1 measuring 0.0076 $g.cm^{-3}$, fitting within the density range of cellulose aerogel, which is known for its lightweight properties, ranging from 0.047 to 0.091 $g.cm^{-3}$[19]. The two samples obtained different

phenomena at coagulation. In contrast to sample AM-0, which has more scattered magnetite in the aerogel, sample AM-1 is made up of two layers that are clearly apparent. This suggests that the magnetic field applied during co-gelation can influence the position of the magnetite, because magnetite itself is ferrimagnetic [20].

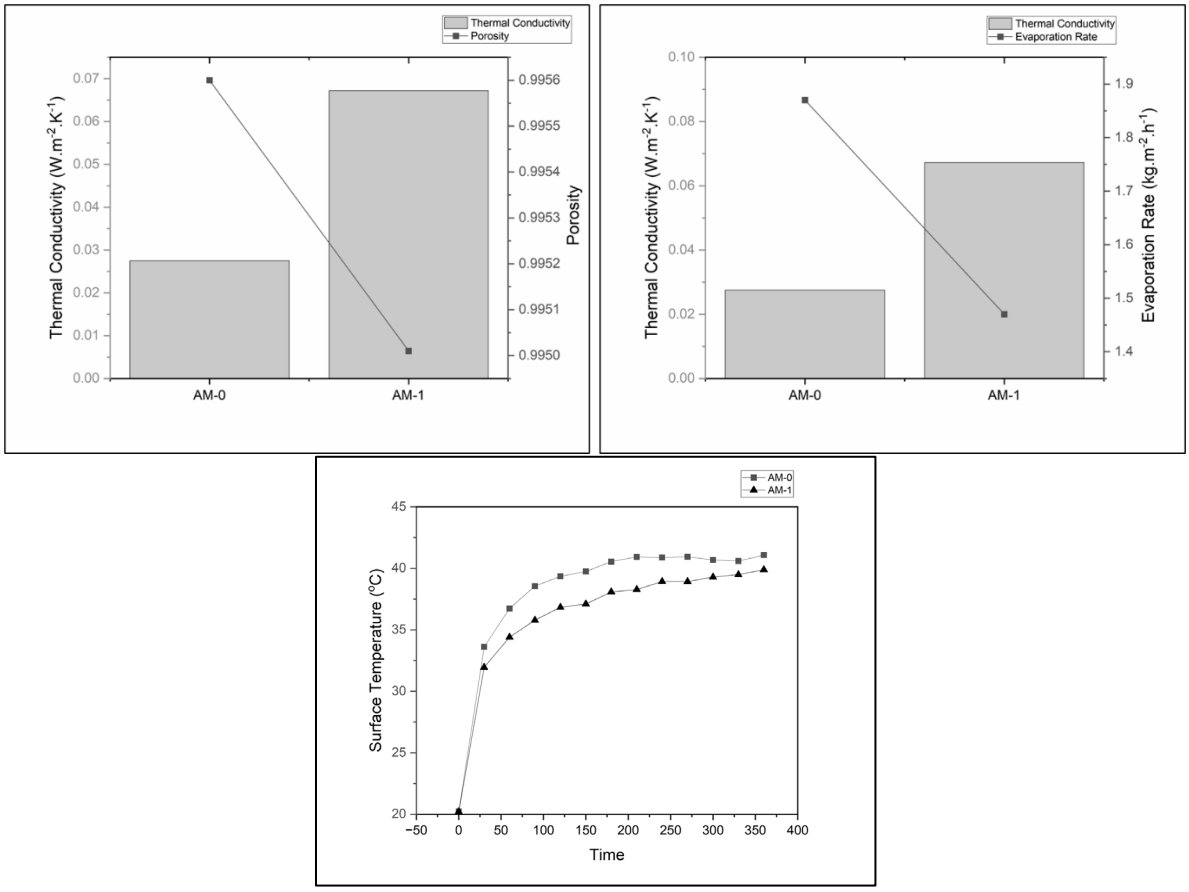

Fig. 6. a) Thermal conductivity vs Porosity, b) Thermal conductivity vs Evaporation Rate, c) Time Dependent Surface Temperature

Both samples have high porosity, each 99.6% for AM-0 and. 99.5% for AM-1 and are suitable with the characteristic of aerogel cellulose. The thermal conductivity values measured from both samples are 0.0275 and 0.0672 $W.m^{-2}.K^{-1}$, falling within the range of insulating materials[21]. High porosity substrates have a lot of void spaces that is filled with air, which has a low thermal conductivity, and making them excellent heat insulating materials[3]. The evaporation rate is influenced by thermal conductivity, as a lower thermal conductivity allows for better heat confinement, hence reducing heat losses during evaporation. This is proved by evaporation rate of AM-0 which is 1.87 $kg.m^{-2}.h^{-1}$ is higher that AM-1 which is 1.47 $kg.m^{-2}.h^{-1}$, which has lower thermal conductivity. Shown in Figure 6(c), surface temperature of AM-0 is constantly higher than AM-1. Because of the more dispersed magnetite at AM-0, sunlight is continuously reflected inside aerogel, raising surface temperature. The rate of evaporation in the solar steam generator will increase as the surface temperature rises.

Conclusion

In conclusion, bilayer solar steam generator that is composed of magnetite (Fe_3O_4) as the photothermal material and cellulose aerogel from coir fibers as the substrate material is promising for SSG with high evaporation rate. It is characterized by low density, low thermal conductivity, and high porosity. As the porosity of aerogel cellulose increases, the thermal conductivity decreases, and the evaporation increases. In addition, deposition of magnetite (Fe_3O_4) is affected by magnetic field that was added at co-gelation. The highest evaporation rate was obtained by AM-0, bilayer aerogel cellulose magnetite without assisted by magnetic at 1.87 $kg.m^{-2}h^{-1}$.

References

[1] Y. Guo and G. Yu, "Engineering Hydrogels for Efficient Solar Desalination and Water Purification," *Accounts Mater. Res.*, vol. 2, no. 5, pp. 374–384, 2021, doi: 10.1021/accountsmr.1c00057.

[2] Y. S. Jun, X. Wu, D. Ghim, Q. Jiang, S. Cao, and S. Singamaneni, "Photothermal Membrane Water Treatment for Two Worlds," *Acc. Chem. Res.*, vol. 52, no. 5, pp. 1215–1225, 2019, doi: 10.1021/acs.accounts.9b00012.

[3] H. Setyawan, J. Juliananda, and W. Widiyastuti, "Engineering Materials to Enhance Light-To-Heat Conversion for Efficient Solar Water Purification," *Ind. Eng. Chem. Res.*, vol. 61, no. 49, pp. 17783–17800, 2022, doi: 10.1021/acs.iecr.2c03170.

[4] H. Ghasemi *et al.*, "Solar steam generation by heat localization," *Nat. Commun.*, vol. 5, 2014, doi: 10.1038/ncomms5449.

[5] C. Song, Z. Jiang, X. Gu, H. Li, and J. Shi, "A bilayer solar evaporator with all-in-one design for efficient seawater desalination," *J. Colloid Interface Sci.*, vol. 616, pp. 709–719, 2022, doi: 10.1016/j.jcis.2022.02.075.

[6] M. Fauziyah, W. Widiyastuti, R. Balgis, and H. Setyawan, "Production of cellulose aerogels from coir fibers via an alkali–urea method for sorption applications," *Cellulose*, vol. 26, no. 18, pp. 9583–9598, 2019, doi: 10.1007/s10570-019-02753-x.

[7] R. Chen *et al.*, "Interfacial solar heating by self-assembled Fe3O4@C film for steam generation," *Mater. Chem. Front.*, vol. 1, no. 12, pp. 2620–2626, 2017, doi: 10.1039/c7qm00374a.

[8] Y. Guo, H. Lu, F. Zhao, X. Zhou, W. Shi, and G. Yu, "Biomass-Derived Hybrid Hydrogel Evaporators for Cost-Effective Solar Water Purification," *Adv. Mater.*, vol. 32, no. 11, 2020, doi: 10.1002/adma.201907061.

[9] T. Wang and Y. Zhao, "Optimization of bleaching process for cellulose extraction from apple and kale pomace and evaluation of their potentials as film forming materials," *Carbohydr. Polym.*, vol. 253, no. August 2020, p. 117225, 2021, doi: 10.1016/j.carbpol.2020.117225.

[10] P. Nurlilasari, W. Widiyastuti, and H. Setyawan, "Novel monopolar arrangement of multiple iron electrodes for the large-scale production of magnetite nanoparticles for electrochemical reactors," *Adv. Powder Technol.*, vol. 31, no. 3, pp. 1160–1168, 2020, doi: 10.1016/j.apt.2019.12.043.

[11] K. O. Reddy, B. Ashok, K. R. N. Reddy, Y. E. Feng, J. Zhang, and A. V. Rajulu, "Extraction and Characterization of Novel Lignocellulosic Fibers From Thespesia Lampas Plant," *Int. J. Polym. Anal. Charact.*, vol. 19, no. 1, pp. 48–61, 2014, doi: 10.1080/1023666X.2014.854520.

[12] M. Kathirselvam, A. Kumaravel, V. P. Arthanarieswaran, and S. S. Saravanakumar, "Isolation and characterization of cellulose fibers from Thespesia populnea barks: A study on physicochemical and structural properties," *Int. J. Biol. Macromol.*, vol. 129, pp. 396–406, 2019, doi: 10.1016/j.ijbiomac.2019.02.044.

[13] J. Cai and L. Zhang, "Rapid dissolution of cellulose in LiOH/urea and NaOH/urea aqueous solutions," *Macromol. Biosci.*, vol. 5, no. 6, pp. 539–548, 2005, doi: 10.1002/mabi.200400222.

[14] L. Alves, B. F. Medronho, F. E. Antunes, A. Romano, M. G. Miguel, and B. Lindman, "On the role of hydrophobic interactions in cellulose dissolution and regeneration: Colloidal aggregates and molecular solutions," *Colloids Surfaces A Physicochem. Eng. Asp.*, vol. 483, pp. 257–263, 2015, doi: 10.1016/j.colsurfa.2015.03.011.

[15] V.A.R. Baldanza *et al.*, "Controlled-release fertilizer based on poly(butylene succinate)/urea /clay and its effect on lettuce growth," *J. Appl. Polym. Sci.*, vol. 135, no. 47, pp. 51–60, 2018, doi: 10.1002/app.46858.

[16] A.D. French, "Idealized powder diffraction patterns for cellulose polymorphs," *Cellulose*, vol. 21, no. 2, pp. 885–896, 2014, doi: 10.1007/s10570-013-0030-4.

[17] C. Wan, Y. Jiao, S. Wei, L. Zhang, Y. Wu, and J. Li, "Functional nanocomposites from sustainable regenerated cellulose aerogels: A review," *Chem. Eng. J.*, vol. 359, pp. 459–475, 2019, doi: 10.1016/j.cej.2018.11.115.

[18] X. Chen, J. Chen, T. You, K. Wang, and F. Xu, "Effects of polymorphs on dissolution of cellulose in NaOH/urea aqueous solution," *Carbohydr. Polym.*, vol. 125, pp. 85–91, 2015, doi: 10.1016/j.carbpol.2015.02.054.

[19] M. Chen, X. Zhang, A. Zhang, C. Liu, and R. Sun, "Direct preparation of green and renewable aerogel materials from crude bagasse," *Cellulose*, vol. 23, no. 2, pp. 1325–1334, 2016, doi: 10.1007/s10570-015-0814-9.

[20] R. Chen, Z. Wu, T. Zhang, T. Yu, and M. Ye, "Magnetically recyclable self-assembled thin films for highly efficient water evaporation by interfacial solar heating," *RSC Adv.*, vol. 7, no. 32, pp. 19849–19855, 2017, doi: 10.1039/c7ra03007j.

[21] F.K.K. Muzaffer A. Karaaslan, John F. Kadla, "Lignin-Based Aerogels," *Lignin Polym. Compos.*, 2016.

[22] Zensu S., Dalimi R. Implementation of 100% electrical vehicle in Bali with the supply of potential Independent solar energy. MECHTA vol 3, no 1, 2022.